Journal of Materials Chemistry A

ROYAL SOCIETY OF CHEMISTRY

PAPER

View Article Online
View Journal | View Issue

Cite this: J. Mater. Chem. A, 2023, 11, 14682

Promotion of photocatalytic hydrogen production by utilization of triplet excited states of organic dyes and adjustment of π–π interactions†

Siwei Liu,[a] Qian Chen,[b] YanTing Chen,[a] Peixuan Lin,[a] Hangyu Zhuzhang,[b] Mengmeng Han,[a] Zhi-An Lan,*[b] Xiong Chen,[b] Xinchen Wang,*[b] Qianqian Li*[a] and Zhen Li*[a]

Received 1st February 2023
Accepted 2nd June 2023

DOI: 10.1039/d3ta00563a

rsc.li/materials-a

Dye/polymeric carbon nitride (PCN) systems exhibit great potential for photocatalytic hydrogen evolution (PHE), due to the broad light-harvesting region and optimized charge separation ability. However, charge recombination due to the unmatched photogenerated carrier lifetimes (ns level) of organic dyes and photocatalytic reaction rates (s level) is a major hindrance, which afforded a big challenge to modulate electronic processes by prolongation of carrier lifetimes of dyes. Herein, the excited triplet states of organic dyes with longer carrier lifetimes (ms level) were employed in PHE systems for the first time, which are stabilized by the adjustment of π–π interactions of conjugation skeletons with alkyl chain engineering. By utilizing the increased isolation effect of alkyl chains, from linear to branched ones with prolonged lengths, higher PHE activities were achieved by branched chain-substituted dyes due to their longer lifetimes, accompanied by the improved phosphorescence properties, and suppressed charge recombination. Accordingly, a relationship among properties of triplet excited states, alkyl chains, and PHE activity has been roughly built, providing valuable information for further promoting PHE activities by adjustment of dye–dye and dye–PCN interactions.

Introduction

Photocatalytic hydrogen evolution (PHE) is an effective solution for the increasingly serious energy and environmental problems.[1–5] Polymeric carbon nitride (PCN) as a representative metal-free semiconductor has been extensively investigated for its appropriate bandgap, high thermal stability, reasonable cost and especially for being nontoxic.[6–11] However, carrier recombination involved in PCN photocatalysts includes undissociated exciton decay and charge recombination, which are a major hindrance limiting photocatalytic activities. Therefore, realization of highly efficient charge generation and separation simultaneously in a PCN system is a fundamental strategy for the potential success of solar-to-hydrogen conversion, but still a great challenge.[12–16] Basically, the incorporation of organic dyes into PCN systems is an efficient strategy to broaden the light harvesting region and optimize the charge separation ability of photocatalysts.[17–22] However, the photogenerated carrier lifetime of organic dyes is usually at the nanosecond (ns) level, as derived from the singlet excited state, while the photocatalytic reaction usually occurs at the second (s) level. The large gaps in time scales of these two key processes in PHE systems usually resulted in severe recombination in the photocatalytic process.[23–27] Thus, it is essential to prolong the excited state lifetimes of organic dyes to improve the PHE performance.[28–30]

According to the basic knowledge of molecular photochemistry, the lifetimes (ms–s levels) of triplet excited states (T_n) are much longer than those (ns–μs levels) of singlet excited states (S_n), for the spin-forbidden transitions to ground states.[31–34] Thus, for organic dyes, the utilization of triplet excited states, instead of the frequently used singlet excited states, to prolong the lifetimes should be an efficient approach to decrease the gaps in the time scales of photogenerated carrier lifetimes and rates of photocatalytic reactions in PHE systems as mentioned above. However, for organic molecules, the triplet excited states are usually unstable, easily dissipated by the non-transition process, and quenched by the moisture and oxygen in the environment, affording a big challenge to stabilize triplet excited states of organic dyes by rational molecular design.[35–39]

According to the basic knowledge of molecular photochemistry, the stable triplet excited states can result in room temperature phosphorescence (RTP) as the radiative transition process, which can be considered as an important parameter to

[a]Hubei Key Lab on Organic and Polymeric Opto-Electronic Materials, TaiKang Center for Life and Medical Sciences, Department of Chemistry, Wuhan University, Wuhan 430072, China. E-mail: lizhen@whu.edu.cn

[b]State Key Laboratory of Photocatalysis on Energy and Environment, College of Chemistry, Fuzhou University, Fuzhou, 350116, China

† Electronic supplementary information (ESI) available. See DOI: https://doi.org/10.1039/d3ta00563a

evaluate the properties of excited excitons as photogenerated carriers. However, until now, RTP properties of organic dyes with strong intramolecular charge transfer (ICT) processes have seldom been reported, due to the narrow energy gap between triplet excited states and ground states, which can largely accelerate the non-radiative transitions according to the energy gap law. Fortunately, in our previous work, the non-radiative transitions could be largely suppressed by the intramolecular O···S interactions, as conformation locks between benzothiadiazole and thiophene moieties, resulting in the persistent RTP emission.[40,41] This indicated that the stability of triplet excited states is highly related to the conformational rigidity. Thus, with rational molecular design, some new organic dyes with RTP properties, especially longer lifetimes, might achieve high efficiencies for PHE activity.

Actually, for dye/PCN systems as photocatalysts, not only the molecules themselves, but the corresponding properties at aggregated states should also be considered, including the intermolecular interactions among organic dyes, as well as the electronic processes between dyes and PCN. Accordingly, the application of organic dyes with RTP properties in PHE systems, should consider all the above points, including light-harvesting ability, photogenerated carrier lifetimes, and molecular packing of dyes on the surface of PCN for efficient electronic transitions. Herein, alkyl chain engineering is employed in organic dyes with a triphenylamine–thiophene–benzothiadiazole–thiophene–triphenylamine skeleton as the D–π–A–π–D structure, including the linear and branched alkyl chains with different lengths, with the aim to adjust the π–π interactions by using the various sizes and shapes. The effective regulation of molecular aggregates resulted in improved RTP properties and PHE performance, and the organic dyes with branched alkyl substitutions (**LI-161**–**LI-165**) demonstrated a higher PHE activity than those (**LI-154**–**LI-158**) with linear ones, due to the larger isolation effect stabilizing the triplet excited states and balancing the electronic transitions at the interface. Moreover, the relationship among molecular structures of organic dyes, RTP properties and PHE activity has been roughly built, and the adjustment of π–π interactions among organic dyes, and in the dye/PCN system is highlighted as the key point. It is the first time that triplet excited states of organic dyes were incorporated into PHE systems, offering an efficient strategy to promote the PHE activity by balancing the electronic transitions.

Results and discussion

Design and synthesis of organic dyes

These organic dyes consist of the same conjugated skeletons with D–π–A–π–D structures, which can result in dual intramolecular charge transfer (ICT) from D to A moieties through the π-bridge, benefiting light-harvesting by the extended absorption spectra and high molar extinction coefficients. Moreover, alkyl chains with different lengths, including linear and branched ones, are linked to tune π–π stacking modes of organic dyes in the aggregated states. Accordingly, the lifetimes of excited states can be modulated by the intersystem crossing (ISC) process and stability of excited triplet states, under different conditions. Also, the electronic transitions between dyes and PCN can be adjusted by the varied π–π interactions, in which alkyl chains can act as the isolation groups to tune the distances between them to some extent. Molecular structures and purity of these compounds are fully confirmed by ^{1}H NMR, ^{13}C NMR, MALDI-TOF(MS), FTIR, and elemental analyses (Fig. S1–S22†). They exhibit good solubility in petroleum ether, chloromethane and other common organic solvents.

Photophysical properties of organic dyes

The absorption spectra of these organic dyes are similar, which can extend to 600 nm due to the strong ICT effect (Fig. 2a), and the molar extinction coefficients are in the range of 1.95–4.10 × 10^4 L mol^{-1} cm^{-1} (Table 1 and Fig. S23†), contributing to the strong light harvesting ability towards sunlight. All of them

Table 1 Photophysical properties of dye molecules

Dye	λ_{abs}[a] [nm]	λ_{onset}[a] [nm]	λ_{onset}[b] [nm]	λ_{em}[c] [nm]	ε[d] [×10^4 L mol^{-1} cm^{-1}]	Φ[e] [%]	τ_{ave}[f] [ns]	E_{0-0}[g] [eV]	E_{HOMO}[h] [eV]	E_{LUMO}[i] [eV]
LI-154	370, 504	602	699	667	4.10	68.47	3.53	1.81	−5.37	−3.56
LI-155	342, 488	584	684	662	1.95	73.84	3.05	1.79	−5.27	−3.48
LI-156	342, 489	586	661	662	2.62	77.25	2.97	1.92	−5.38	−3.46
LI-157	342, 489	586	680	662	2.94	66.80	6.01	1.85	−5.16	−3.31
LI-158	343, 490	583	680	663	2.46	71.29	5.48	1.91	−5.32	−3.41
LI-161	342, 489	580	670	659	3.04	80.52	3.35	1.89	−5.01	−3.12
LI-162	342, 489	585	672	657	4.50	83.69	6.33	1.85	−4.55	−2.70
LI-163	341, 490	583	671	657	3.23	89.63	6.31	1.85	−4.38	−2.53
LI-164	341, 489	582	647	656	3.06	82.78	3.02	2.00	−4.37	−2.37
LI-165	342, 489	583	620	656	3.25	95.01	2.40	2.09	−4.71	−2.62

[a] UV-vis absorption spectra of dyes in CH_2Cl_2 solution at a concentration of 1 × 10^{-5} mol L^{-1}. [b] UV-vis DRS absorption spectra of dyes (solid state, the results of semisolid **LI-164** and **LI-165** were measured by using thin films). [c] The PL spectra of dyes in CH_2Cl_2 solution at a concentration of 1 × 10^{-5} mol L^{-1}. [d] Molar extinction coefficient of dyes in CH_2Cl_2 solution. [e] Photoluminescence quantum yield of dyes in the solid state. [f] PL lifetimes of dyes in the solid state. [g] The optical band gap of dyes as measured by using Tauc-plots. [h] HOMO energy levels as calculated by UPS. [i] LUMO energy levels as calculated by using $E_{LUMO} = E_{HOMO} - E_{0-0}$.

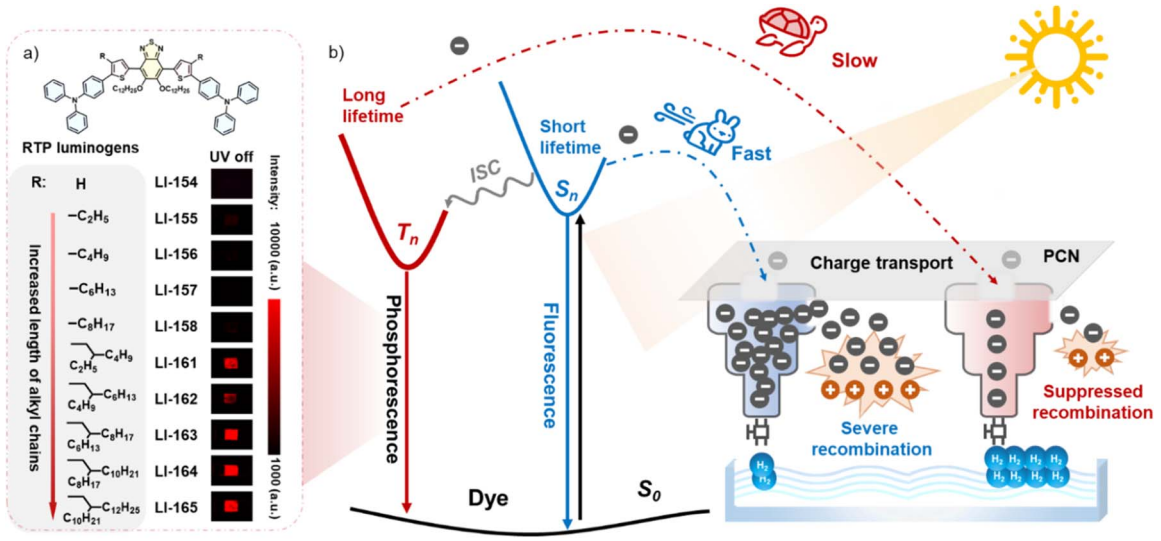

Fig. 1 (a) The molecular structures of organic dyes (**LI-154**–**LI-158** and **LI-161**–**LI-165**) with different alkyl chains as substituents, and the corresponding RTP imaging captured by using a chemiluminescence imager. (b) Schematic diagram of electronic transition processes in a photocatalytic hydrogen evolution system, including sunlight-harvesting, charge separation, exciton migration and hydrogen evolution.

exhibit bright red fluorescence in CH_2Cl_2 solution at room temperature, and the emission wavelengths are mainly located at 660 nm (Fig. 2b, Fig. S24 and S25†). Once the temperature is cooled to 77 K, the blue-shifts of fluorescence emission wavelengths are obvious, mainly located at 590 nm with orange emission (Fig. S26†). Meanwhile, the emission peaks emerged at about 800 nm, which should be ascribed to phosphorescence emission. It can be further confirmed by their phosphorescence spectra under the same conditions, in which two peaks at about 580 nm and 800 nm can be observed (Fig. S27†).

When these organic dyes aggregate in the solid or oil state, light harvesting regions can further extend to about 680 nm (Fig. S28†), mainly due to the possible π–π interactions at the aggregated states. Moreover, with the volumes of alkyl chains enlarged by the increased lengths, and the varied shapes from linear to branched ones, the absorption edges demonstrate obvious blue-shifts from 700 nm to 620 nm gradually. Also, fluorescence spectra exhibit blue-shifts of about 60 nm due to the modification of alkyl chains with enlarged sizes (Fig. 2d), and the lifetimes of excited singlet states are at the same level (Fig. 2e and Table S1†). It may be related to the varied molecular configurations, which can be optimized by density functional theory (DFT) calculations using the Gaussian 09 program.[42] Accordingly, molecular configurations become twisted with prolonged alkyl chains, as confirmed by the increased dihedral angles between the benzothiadiazole group and thiophene from 1.55–4.69° (**LI-155**–**LI-158**) to 10.71–13.93° (**LI-161**–**LI-165**) (Fig. S29†). Generally, strong π–π interactions can quench the fluorescence emission in most cases, and thus, their photoluminescence quantum yields increase from 68.47% (**LI-154**) to 95.01% (**LI-165**) with the efficient suppression of π–π interactions by the increased isolation effect of alkyl chains (Fig. 2c).

The adjustable molecular aggregates by alkyl chains can further promote the ISC process, contributing to the generation of excited triplet states, as proved by the obvious phosphorescence images (captured by using the chemiluminescence imager) of dye **LI-161**–**LI-165** (Fig. 1a and S30†). Accordingly, the phosphorescence spectra at room temperature

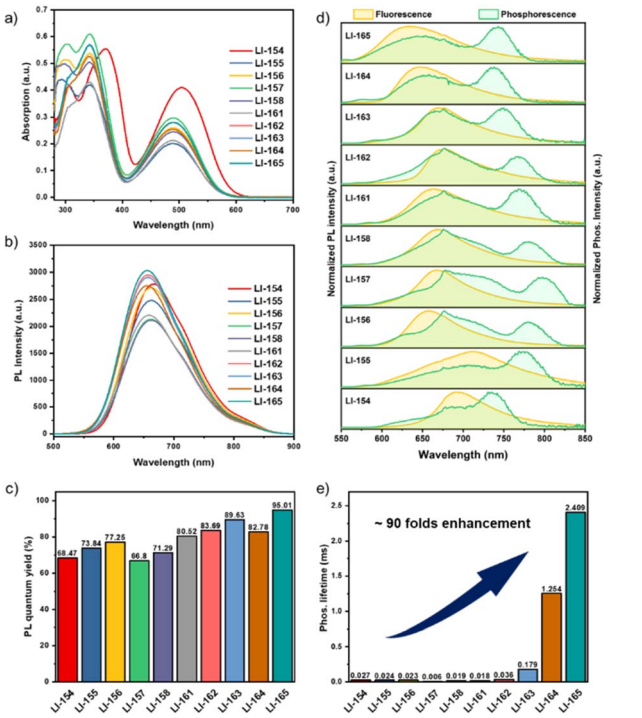

Fig. 2 (a) UV-vis absorption spectra of organic dyes in CH_2Cl_2 dilute solution (concentration: 1×10^{-5} mol L^{-1}). (b) Fluorescence spectra of organic dyes in CH_2Cl_2 dilute solution (concentration: 1×10^{-5} mol L^{-1}) (λ_{ex}: 430 nm). (c) Photoluminescence quantum yields (PLQYs) of organic dyes in the solid state. (d) Photoluminescence (yellow line) and room temperature phosphorescence (green line) spectra of organic dyes in the solid state. (e) Phosphorescence lifetimes of organic dyes in the solid state.

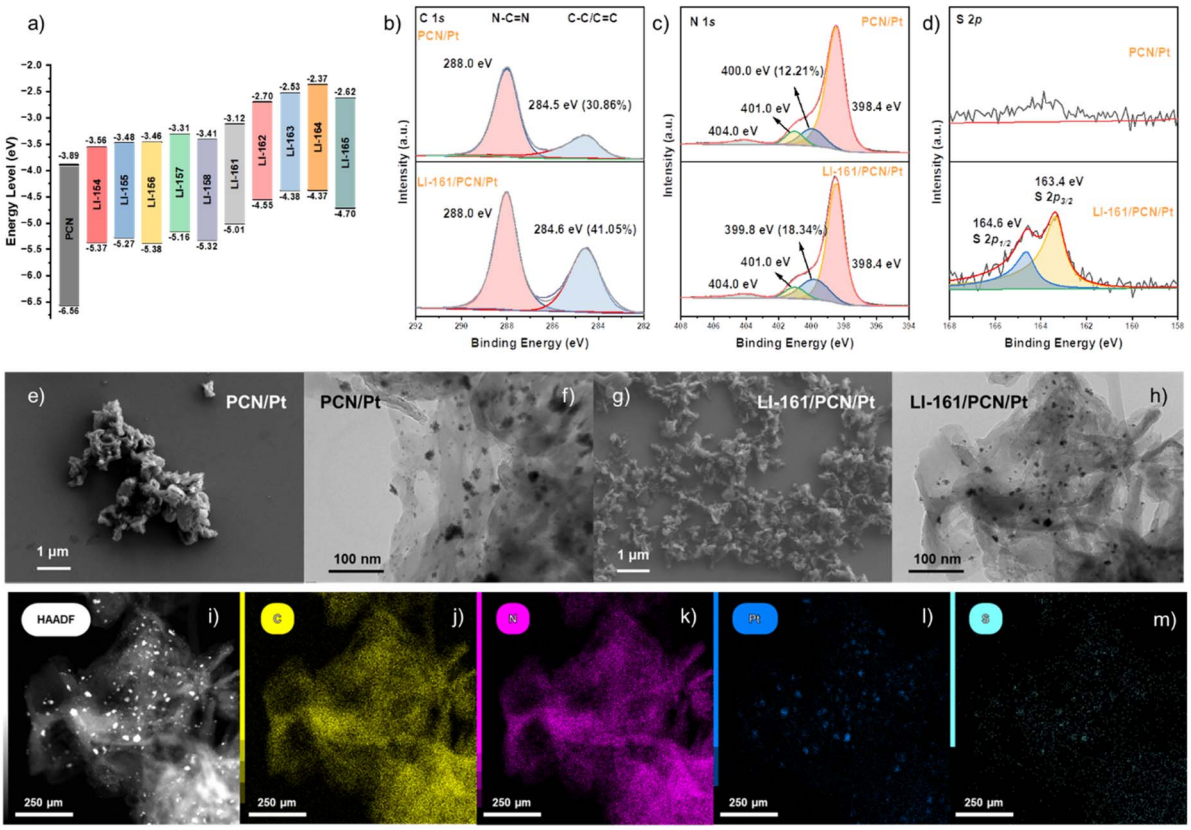

Fig. 3 (a) Energy-level diagram of PCN and organic dyes. (b–d) High-resolution XPS spectra of PCN/Pt and dye/PCN/Pt: (b) C 1s, (c) N 1s, and (d) S 2p. (e–h) SEM and TEM images of PCN/Pt (e and f) and **LI-161**/PCN/Pt (g and h). (i) HAADF-STEM image of **LI-161**/PCN/Pt. (j–m) Elemental mapping images of **LI-161**/PCN/Pt with elemental distributions of (j) C, (k) N, (l) Pt and (m) S.

show two emission peaks at about 680 nm and 735–790 nm, respectively (Fig. 2d and S31†). The phosphorescence lifetimes have a ~90 fold increase with the prolonged alkyl chains, ranging from 0.027 ms (**LI-154**) to 2.409 ms (**LI-165**) (Fig. 2e, S32 and Table S2†). It is the first time that near IR phosphorescence was achieved by organic materials with a single component, mainly due to the restriction of molecular motions by the intramolecular O···S interactions between thiophene and the alkoxy chains being linked to benzothiadiazole, and the inhibition of π–π interactions by alkyl chains with steric hindrance.

Dye/PCN/Pt heterojunction systems

Subsequently, dye/PCN/Pt heterojunction systems are fabricated by two steps: first, a PCN/Pt system is formed by photodeposition of Pt on the surface of PCN, and then, dye (2 wt%) and PCN/Pt are mixed and dispersed in $CHCl_3$ solvent to prepare the heterojunction systems by using rotary evaporators. FTIR spectroscopy (Fig. S33†) and XRD (Fig. S34†) show that the structure of PCN has not been damaged during these processes. The resultant heterojunction systems exhibit a broad absorption region extended to 700 nm, mainly due to the strong light-harvesting ability of organic dyes (Fig. S35†). In order to further investigate the dispersive forms of organic dyes, the absorption spectra of dye/PCN/Pt and organic dyes have been compared. The dye/PCN/Pt systems demonstrate red-shifted absorption, compared to that of organic dyes in diluted solution with isolated state. It is mainly due to the possible dye aggregation at the surface of PCN, which can be partially proved by the red-shifted absorption spectra of organic dyes in the solid/film states. The energy levels of organic dyes match well with those of PCN (Fig. 3a, S36 and S37†), which possess sufficient driving force to complete the efficient electron injection from organic dyes into PCN.

The surface topography of each heterojunction system has been characterized by XPS. As shown in Fig. 3b, the high-resolution C 1s spectra can be mainly resolved into two peaks, where the peak at about 288.0 eV corresponds to the N–C=N bond and the peak at about 284.5 eV corresponds to the C–C/C=C peak (Fig. S38a†).[43,44] Compared to the PCN/Pt system, the ratio of C–C/C=C bonds of each dye/PCN/Pt system increases significantly, which is brought about by the additional aromatic moieties in these dyes (Table S3†). In the high-resolution S 2p spectra (Fig. 3d and S38c†), two characteristic peaks can be found at about 164.5 eV and 163.5 eV, which comes from the benzothiazole moieties of organic dyes.[45] In the high-resolution N 1s spectra (Fig. 3c and S38b†), the four peaks of PCN/Pt can be assigned to π excitations (about 404 eV), quaternary N (C–NH) (about 401 eV), tertiary N (N–$(C)_3$) (about 400 eV) and sp^2-hybridized aromatic N (C=N–C) (about 398 eV), respectively.[46] The higher ratios of dye/PCN/Pt at about 400 eV

than that of PCN/Pt are assigned to C–N bonds in the TPA unit of organic dyes. Meanwhile, the slightly lower binding energies of dye/PCN/Pt systems than that of PCN/Pt (Table S4†), suggests the increased electron density of the N atom after the incorporation of organic dyes, which is mainly related to the possible charge transfer process from organic dyes to PCN through intermolecular π–π interactions.[47]

Scanning electron microscope (SEM) and transmission electron microscope (TEM) images clarify that the deposited Pt particles are uniformly distributed on the surface of PCN as small particles (Fig. S39†), and no specific structure of dyes is observed in the dye/PCN/Pt sample for a low concentration (2 wt%) (Fig. S40†). However, this can be observed in the elemental mapping images of the **LI-161**/PCN/Pt system as an example (Fig. 3i–m). The brightest points in the HAADF-STEM picture (Fig. 3i) correspond to Pt with the highest atomic number among the C, N, O and S elements, which is consistent with the distribution of Pt (Fig. 3l). The part with slightly weaker brightness than that of Pt, corresponded to the S element in the benzothiazole moiety, indicating the good dispersion of **LI-161** on the surface of PCN. It can be further confirmed by the distribution diagram of the S element (Fig. 3m). Also, compared to PCN/Pt, VB XPS of dye/PCN/Pt shows a slight offset (Fig. S41†), mainly due to the distribution of dye on the surface of PCN. It is confirmed by hydrophobic properties of dye/PCN/Pt systems with water contact angles of about 140° (Fig. S42†).

Photocatalytic hydrogen production and stability

The hydrogen evolution activities of dye/PCN/Pt systems as photocatalysts are evaluated with triethanolamine (TEOA) as the sacrificial agent, under visible-light irradiation ($\lambda \geq 420$ nm). Taking the **LI-161**/PCN/Pt system as an example (Fig. 4a), with the increased proportion of dye from 1.0% to 3.0% (wt%), the photocatalytic hydrogen evolution (PHE) rates first increased, and then decreased. The highest hydrogen evolution is achieved at a dye content of 2.0%, which is fixed as the optimal concentration of organic dyes in the following PHE experiments. As the reference, PCN/Pt exhibits low H_2 generation activity with a rate of 16.1 μmol h^{-1} (Fig. 4b). After modification by these organic dyes, the PHE activity was enhanced largely by the strong light-harvesting ability and efficient charge separation. In these dye/PCN/Pt systems, organic dyes bearing branched alkyl chains (**LI-161**–**LI-165**) and/or long linear chains (**LI-158**), exhibit better PHE performance (320.4–593.9 μmol h^{-1}) than those (**LI-154**–**LI-157**) bearing short linear chains (115.3–281.2 μmol h^{-1}), and dye **LI-161** based photocatalysts achieve the highest performance of 593.9 μmol h^{-1}. It may be related to the longer lifetime of excited triplet states, as well as the efficient charge transfer between dyes and PCN. The apparent quantum yields (AQYs) of **LI-161**/PCN/Pt are over 7.0% in the broad region of 420–520 nm (Fig. 4c and Table S4†), and reaches the highest yield of 10.87% at 450 nm, further confirming the strong light harvesting ability and balanced charge

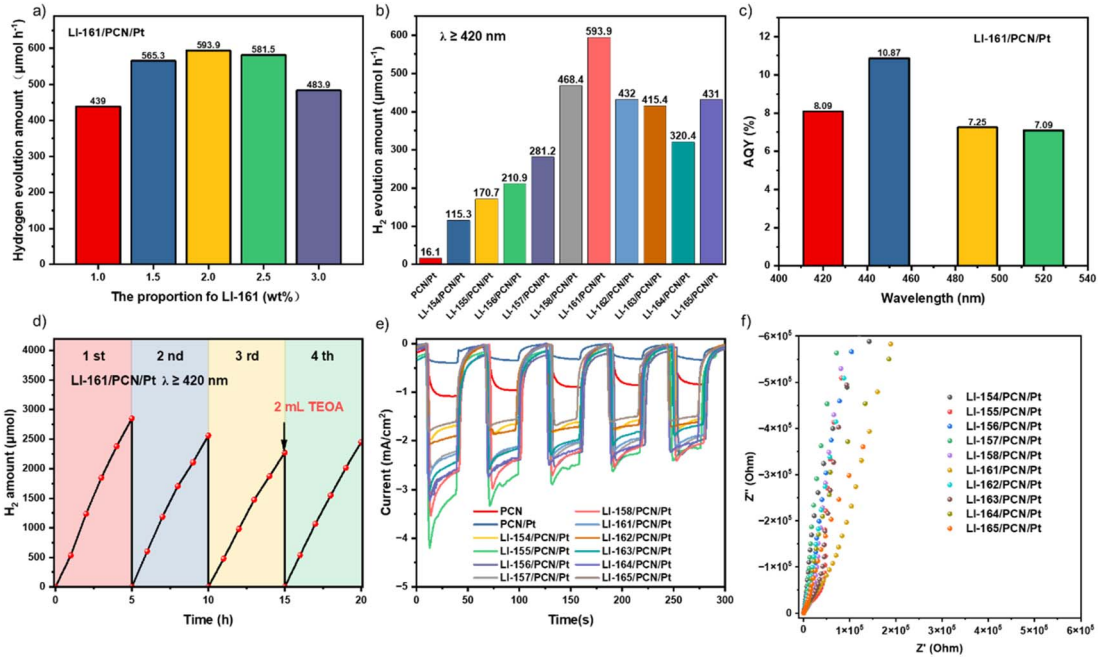

Fig. 4 (a) The photocatalytic hydrogen evolution activities of the **LI-161**/PCN/Pt system with different proportions of dyes under visible-light irradiation (50 mg photocatalyst, 10 mL TEOA, 100 mL H_2O, and a 300 W Xe lamp with a cut-off filter $\lambda \geq 420$ nm). (b) The photocatalytic hydrogen evolution activities of PCN/Pt and dye/PCN/Pt systems under visible-light irradiation (50 mg photocatalyst, 10 mL TEOA, 100 mL H_2O, and a 300 W Xe lamp with a cut-off filter $\lambda \geq 420$ nm). (c) Calculated apparent quantum yields (AQY) of **LI-161**/PCN/Pt under illumination at different wavelengths. (d) Cycling measurements of **LI-161**/PCN/Pt under visible-light irradiation (50 mg photocatalyst, 10 mL TEOA, 100 mL H_2O, and a 300 W Xe lamp with a cut-off filter $\lambda \geq 420$ nm). (e) Transient photocurrent densities of PCN, PCN/Pt and dye/PCN/Pt electrodes in 0.5 M Na_2SO_4 solution under the irradiation of visible light ($\lambda \geq 420$ nm). (f) Electrochemical impedance spectra (EIS) of PCN, PCN/Pt and dye/PCN/Pt in 0.5 M Na_2SO_4 solution under the irradiation of visible light ($\lambda \geq 420$ nm) (Nyquist plots).

transitions for hydrogen evolution. Subsequently, four cycles of the photocatalysis reaction were tested to measure the stability of the **LI-161**/PCN/Pt system: in the first and second cycles, it remains nearly unchanged; however, it demonstrates a slight decrease from 569.7 μmol h^{-1} to 453.8 μmol h^{-1} in the third cycle, and finally, it increased to 489.5 in the fourth cycle after TEOA supplementation (Fig. 4d).

Discussion

The varied PHE activities with alkyl chain engineering indicate that the electronic transition process can be adjusted by the isolation effect of alkyl chains with different shapes. Since they exhibit a similar light-harvesting ability for the same conjugated skeletons, the differences are mainly related to the properties of triplet excited states, as illustrated by the RTP effect, and the charge transfer/recombination process. For the electronic transitions at the interface, an improved transient photocurrent response can be observed by the addition of organic dyes (Fig. 4e) to different degrees; however, their differences decreased with the increased number of cycles. Broadly, the transient photocurrents of PHE systems based on organic dyes (**LI-161**–**LI-165**) with branched alkyl chains are higher than those of dyes bearing linear chains (**LI-154**–**LI-158**). This trend can be further confirmed by the results of electrochemical impedance spectroscopy (EIS) under light irradiation. As shown in Fig. 4f, **LI-161**/PCN/Pt–**LI-165**/PCN/Pt exhibit smaller semicircular curves than those of **LI-154**/PCN/Pt–**LI-158**/PCN/Pt in Nyquist plots, indicating the lower transmission impedance and more efficient charge transfer processes, as further confirmed by EIS under a bias of −1.2 V (*vs.* RHE) with **LI-154**/PCN/Pt, **LI-155**/PCN/Pt, **LI-161**/PCN/Pt and **LI-165**/PCN/Pt as the representative samples (Fig. S43†). Also, transient open-circuit voltage decay (OCVD) measurements show that **LI-161**/PCN/Pt electrodes have a higher photo-responsive voltage and slower photovoltage attenuation during light cycling, than those of **LI-154**/PCN/Pt and **LI-155**/PCN/Pt electrodes (Fig. S44†), mainly due to the different intermolecular interactions between dye and PCN, as well as the properies of excited states of dyes.

The dye/PCN interactions can be investigated by PL spectra in various states (Fig. S45 and Table S5†). Under UV irradiation (375 nm), PCN exhibits bright emission with a maximum wavelength of 450 nm, and an average lifetime of 7.74 ns. With photo-deposition of Pt, the resultant PCN/Pt system demonstrates decreased emission intensity and a slightly shorter lifetime (6.97 ns) (Fig. S46†). Then, after the addition of organic dyes, there are no new PL emission peaks in the PL spectra of dye/PCN/Pt systems, in addition to emission from the individual PCN/Pt and dyes. The emission intensities further decrease, and lifetimes shorten to 5.85–6.28 ns. These results indicate the efficient charge transfer among PCN, Pt and organic dyes, which can be further confirmed by the quenching effect of PCN on the PL emission (about 670 nm) of organic dyes (Fig. S47, S48 and Table S6†).

With the aim to clarify the direction of charge transfer in PHE systems, the work functions of dye, PCN and PCN/Pt were measured by UPS, which was defined as the minimum amount of thermodynamic work required to remove an electron from a solid to a point in the vacuum immediately outside the solid surface. After photodeposition of Pt on PCN, the work function increased largely from 3.74 eV (PCN) to 5.69 eV (PCN/Pt), which was higher than that of organic dyes, with **LI-161** as an example (4.31 eV) (Fig. S49†). It indicated that the electrons preferred to transfer from dye to PCN/Pt. Thus, dye/PCN/Pt for photocatalytic hydrogen production is likely to be a type II heterojunction system, and not a Z-scheme heterojunction one (Fig. S50†).[48,49] The detailed charge transfer processes are as follows: under excitation by visible light ($\lambda \geq 420$ nm), electronic transitions occur from the excited states of organic dyes to the conduction band of PCN, and the electrons can be further captured by Pt nanoparticles to produce H_2 from water. Meanwhile, both PCN and organic dyes can be regenerated by the sacrificial reagent (TEOA) with hole transitions.

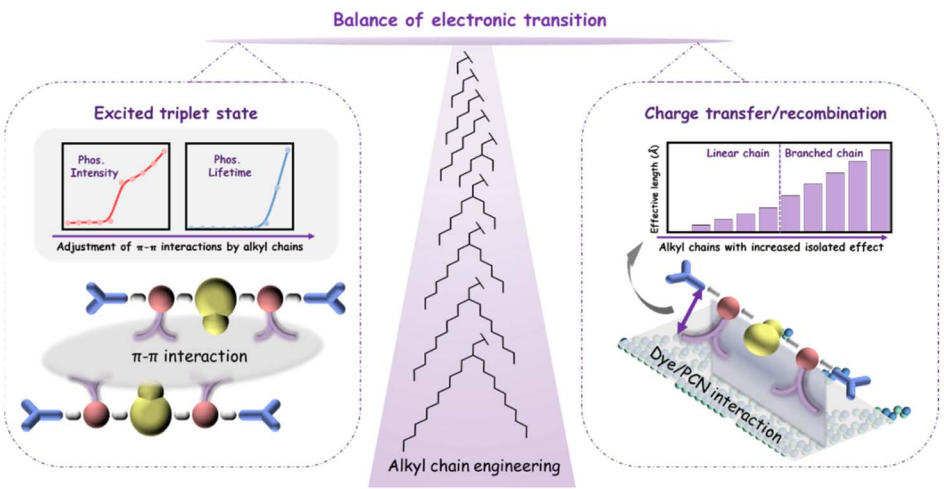

Fig. 5 The balance of electronic transition processes in PHE systems by the adjustable properties of excited triplet states, as well as the charge transfer/recombination at the interface by side-chain engineering.

The possible interactions of organic dyes and TEOA have been investigated by PL spectra and lifetime of dyes in water and 10% TEOA aqueous solution. The emission intensity demonstrated minor changes, and there was a tiny difference in the fluorescence lifetimes with the addition of TEOA (Fig. S51 and S52†). Thus, the excited state of organic dyes cannot be efficiently quenched by TEOA, further confirming the direction of charge transfer.

Since the conjugated skeleton of organic dyes is a planar π system for intramolecular O···S interactions, the dye/PCN interactions were mainly π–π interactions, which could affect the charge transfer and recombination processes at the interface. Theoretically, the strong π–π interactions with close distances can promote both charge transfer and recombination, and *vice versa*. Thus, the modest π–π interactions with suitable distances can balance the charge transfer and recombination to promote the efficient PHE process. Accordingly, alkyl chain engineering of organic dyes can well-tune the π–π distances through their isolation effect. For linear alkyl chains, the isolation effect is usually weak for short effective lengths (1.28–4.34 Å), and it can be largely increased to 6.60–14.65 Å by the incorporation of branched alkyl chains, indicating the larger isolation effect (Fig. S53†). Among them, **LI-161** with the modest isolation effect results in well-balanced electronic transitions at the interface. Combined with the prolonged lifetime of excited states with RTP emission, the carrier generation and transition process in PHE systems is optimized by the modest π–π interactions, contributing to the highest PHE activity (Fig. 5).

Conclusions

Organic dyes with D–π–A–π–D structures are applied in PHE systems by forming dye/PCN heterojunction systems. Moreover, the dye–dye and dye–PCN interactions can be well-tuned by alkyl chain engineering, to solve the unmatched electronic transitions at the interface. With the increased sizes of alkyl chains from linear to branched ones, the RTP effect of organic dyes can be observed due to the stabilization of excited triplet states by the efficient suppression of π–π interactions with an increased isolation effect, resulting in the prolonger photogenerated carrier lifetimes of organic dyes. This is the first time that the RTP properties of organic dyes are introduced into PHE systems. Combined with the balance of charge transfer and recombination by the adjustment of dye–PCN interactions, improved PHE activity was achieved by the well-matched electronic processes. Thus, these findings afforded an efficient strategy to promote the development of PHE systems by the modulation of excited states of organic dyes and dye/PCN interactions.

Author contributions

Q. L. and Z. L. conceived the project. S. L. synthesized the organic compounds and performed all the measurements. Q. C. and P. L performed part of the photocatalytic test. Y. C. recorded part of the photoluminescence spectra and lifetimes. H. Z. helped to synthesize polymeric carbon nitride. M. H. performed the DFT calculations. Z.-A. L., X. C. and X. W. provided the platform for the photocatalytic test. Q. L. and Z. L. discussed and revised the manuscript.

Conflicts of interest

There are no conflicts to declare.

Acknowledgements

This work was supported by the National Natural Science Foundation of China (22122504, 22235006, and 51973162), Foundation of Hubei Scientific Committee (2022BAA015) and Wuhan City (whkxjsj014).

References

1 Y. Fang, Y. Zheng, T. Fang, Y. Chen, Y. Zhu, Q. Liang, H. Sheng, Z. Li, C. Chen and X. Wang, *Sci. China: Chem.*, 2020, **63**, 149–181.
2 T. Hisatomi, J. Kubota and K. Domen, *Chem. Soc. Rev.*, 2014, **43**, 7520–7535.
3 Y. Fang, Y. Hou, X. Fu and X. Wang, *Chem. Rev.*, 2022, **122**, 4204–4256.
4 D. Jiang, *Chem*, 2020, **6**, 2461–2483.
5 S. Xiang, A. Khan, Z. Zhou, B. He, X. Wang, B. Wang and Q. Weng, *J. Mater. Chem. A*, 2022, **10**, 24345–24352.
6 X. Wang, K. Maeda, A. Thomas, K. Takanabe, G. Xin, J. M. Carlsson, K. Domen and M. Antonietti, *Nat. Mater.*, 2009, **8**, 76–82.
7 F. Guo, B. Hu, C. Yang, J. Zhang, Y. Hou and X. Wang, *Adv. Mater.*, 2021, **33**, 2101466.
8 W.-J. Ong, L.-L. Tan, Y. H. Ng, S.-T. Yong and S.-P. Chai, *Chem. Rev.*, 2016, **116**, 7159–7329.
9 B.-X. Zhou, S.-S. Ding, Y. Wang, X.-R. Wang, W.-Q. Huang, K. Li and G.-F. Huang, *Nanoscale*, 2020, **12**, 6037–6046.
10 Y. Si, Z. Lv, L. Lu, M. Liu, Y. Wen, Y. Chen, H. Jin, J. Liu and W. Song, *Appl. Surf. Sci.*, 2019, **491**, 236–244.
11 N. Tian, H. Huang, X. Du, F. Dong and Y. Zhang, *J. Mater. Chem. A*, 2019, **7**, 11584–11612.
12 L. Xu, B. Tian, T. Wang, Y. Yu, Y. Wu, J. Cui, Z. Cao, J. Wu, W. Zhang, Q. Zhang, J. Liu, Z. Li and Y. Tian, *Energy Environ. Sci.*, 2022, **15**, 5059–5068.
13 X. Chen, J. Wang, Y. Chai, Z. Zhang and Y. Zhu, *Adv. Mater.*, 2021, **33**, 2007479.
14 J. Jing, J. Yang, W. Li, Z. Wu and Y. Zhu, *Adv. Mater.*, 2022, **34**, 2106807.
15 M. Liu, Y. Jiao, J. Qin, Z. Li and J. Wang, *Appl. Surf. Sci.*, 2021, **541**, 148558.
16 Q. Zhang, J. Chen, H. Che, P. Wang, B. Liu and Y. Ao, *ACS Mater. Lett.*, 2022, **4**, 2166–2186.
17 F. Yu, Z. Wang, S. Zhang, K. Yun, H. Ye, X. Gong, J. Hua and H. Tian, *Appl. Catal., B*, 2018, **237**, 32–42.
18 K. Li, L. Wang, Z. Chen, X. Yang, Y.-X. Yu, W.-D. Zhang, Y. Wang, Y. Shi, K. P. Loh and Q.-H. Xu, *Adv. Funct. Mater.*, 2020, **30**, 2005106.
19 S. Min and G. Lu, *J. Phys. Chem. C*, 2012, **116**, 19644–19652.

20 L. Xu, B. Tian, T. Wang, Y. Yu, Y. Wu, J. Cui, Z. Cao, J. Wu, W. Zhang, Q. Zhang, J. Liu, Z. Li and Y. Tian, *Energy Environ. Sci.*, 2022, **15**, 5059–5068.
21 X. Liu, Y. Du, Y. Zhao, X. Song, X. Jing, L. Yu and M. Sun, *Appl. Catal., B*, 2022, **312**, 121401.
22 F. Yu, Z. Wang, S. Zhang, H. Ye, K. Kong, X. Gong, J. Hua and H. Tian, *Adv. Funct. Mater.*, 2018, **28**, 1804512.
23 K. Li and W.-D. Zhang, *Small*, 2018, **14**, 1703599.
24 L. Guo, Y. Niu, S. Razzaque, B. Tan and S. Jin, *ACS Catal.*, 2019, **9**, 9438–9445.
25 Z. Hua, X. Zhang, Q. Yin, X. Liu, X. Jiang, Z. Chen, X. Yang, F. Huang and Y. Cao, *Nano Energy*, 2019, **60**, 775–783.
26 J. Fu, Z. Mo, M. Cheng, F. Xu, Y. Song, X. Ding, Z. Chen, H. Chen, H. Li and H. Xu, *Colloids Surf., A*, 2020, **589**, 124397.
27 E. Jin, K. Geng, S. Fu, S. Yang, N. Kanlayakan, M. A. Addicoat, N. Kungwan, J. Geurs, H. Xu, M. Bonn, H. I. Wang, J. Smet, T. Kowalczyk and D. Jiang, *Chem*, 2021, **7**, 3309–3324.
28 X. Zhang, K. Geng, D. Jiang and G. D. Scholes, *J. Am. Chem. Soc.*, 2022, **144**, 16423–16432.
29 H. Ye, Z. Wang, F. Yu, S. Zhang, K. Kong, X. Gong, J. Hua and H. Tian, *Appl. Catal., B*, 2020, **267**, 118577.
30 Y. Qian, D. Li, Y. Han and H.-L. Jiang, *J. Am. Chem. Soc.*, 2020, **142**, 20763–20771.
31 Q. Li and Z. Li, *Acc. Chem. Res.*, 2020, **53**, 962–973.
32 Q. Li and Z. Li, *Sci. China Mater.*, 2020, **63**, 177–184.
33 Y. Tian, J. Yang, Z. Liu, M. Gao, X. Li, W. Che, M. Fang and Z. Li, *Angew. Chem., Int. Ed.*, 2021, **60**, 20259–20263.
34 Q. Liao, Q. Gao, J. Wang, Y. Gong, Q. Peng, Y. Tian, Y. Fan, H. Guo, D. Ding, Q. Li and Z. Li, *Angew. Chem., Int. Ed.*, 2020, **59**, 9946–9951.
35 Y. Gao, Q. Liao, M. Li, M. Han, A. Huang, Q. Dang, Q. Li and Z. Li, *J. Phys. Chem. Lett.*, 2022, **13**, 3251–3260.
36 X. Zhang, J. Liu, B. Chen, X. He, X. Li, P. Wei, P. F. Gao, G. Zhang, J. W. Y. Lam and B. Z. Tang, *Matter*, 2022, **5**, 3499–3512.
37 Z. Cong, M. Han, Y. Fan, Y. Fan, K. Chang, L. Xiao, Y. Zhang, X. Zhen, Q. Li and Z. Li, *Mater. Chem. Front.*, 2022, **6**, 1606–1614.
38 Z. Wang, Y. Zheng, Y. Su, L. Gao, Y. Zhu, J. Xia, Y. Zhang, C. Wang, X. Zheng, Y. Zhao, C. Yang and Y. Li, *Sci. China Mater.*, 2022, **65**, 2160–2168.
39 S. Xiang, C. Han, C. Shu, C. Zhang and J. Jiang, *Sci. China Mater.*, 2022, **65**, 422–430.
40 S. Liu, P. Lin, M. Wu, Z.-A. Lan, H. Zhuzhang, M. Han, Y. Fan, X. Chen, X. Wang, Q. Li and Z. Li, *Appl. Catal., B*, 2022, **309**, 121257.
41 Y. Fan, S. Liu, M. Wu, L. Xiao, Y. Fan, M. Han, K. Chang, Y. Zhang, X. Zhen, Q. Li and Z. Li, *Adv. Mater.*, 2022, **34**, 2201280.
42 M. J. Frisch, G. W. Trucks, H. B. Schlegel, G. E. Scuseria, M. A. Robb, J. R. Cheeseman, G. Scalmani, V. Barone, B. Mennucci, G. A. Petersson, H. Nakatsuji, M. Caricato, X. Li, H. P. Hratchian, A. F. Izmaylov, J. Bloino, G. Zheng, J. L. Sonnenberg, M. Hada, M. Ehara, K. Toyota, R. Fukuda, J. Hasegawa, M. Ishida, T. Nakajima, Y. Honda, O. Kitao, H. Nakai, T. Vreven, J. A. Montgomery Jr, J. E. Peralta, F. Ogliaro, M. Bearpark, J. J. Heyd, E. Brothers, K. N. Kudin, V. N. Staroverov, T. Keith, R. Kobayashi, J. Normand, K. Raghavachari, A. Rendell, J. C. Burant, S. S. Iyengar, J. Tomasi, M. Cossi, N. Rega, J. M. Millam, M. Klene, J. E. Knox, J. B. Cross, V. Bakken, C. Adamo, J. Jaramillo, R. Gomperts, R. E. Stratmann, O. Yazyev, A. J. Austin, R. Cammi, C. Pomelli, J. W. Ochterski, R. L. Martin, K. Morokuma, V. G. Zakrzewski, G. A. Voth, P. Salvador, J. J. Dannenberg, S. Dapprich, A. D. Daniels, O. Farkas, J. B. Foresman, J. V. Ortiz, J. Cioslowski, and D. J. Fox, *Gaussian 09, Revision D.01*, Gaussian, Inc., Wallingford CT, 2013.
43 W. Yan, Z. Han, B. Phung, F. Faupel and K. Ostrikov, *Materials*, 2014, **7**, 563–575.
44 J. Cai, J. Huang, S. Wang, J. Iocozzia, Z. Sun, J. Sun, Y. Yang, Y. Lai and Z. Lin, *Adv. Mater.*, 2019, **31**, 1806314.
45 J. Chen, C.-L. Dong, D. Zhao, Y. Huang, X. Wang, L. Samad, L. Dang, M. Shearer, S. Shen and L. Guo, *Adv. Mater.*, 2017, **29**, 1606198.
46 J. Liu, Y. Liu, N. Liu, Z. Han, X. Zhang, H. Huang, Y. Lifshitz, S.-T. Lee, J. Zhong and Z. Kang, *Science*, 2015, **347**, 970–974.
47 Y. Zheng, Y. Jiao, Y. H. Zhu, L. H. Li, Y. Han, Y. Chen, A. J. Du, M. Jaroniec and S. Z. Qiao, *Nat. Commun.*, 2014, **5**, 3783.
48 R. Kuriki, C. S. K. Ranasinghe, Y. Yamazaki, A. Yamakata, O. Ishitani and K. Maeda, *J. Phys. Chem. C*, 2018, **122**, 16795–16802.
49 R. Kuriki, H. Matsunaga, T. Nakashima, K. Wada, A. Yamakata, O. Ishitani and K. Maeda, *J. Am. Chem. Soc.*, 2016, **138**, 5159–5170.